J. Mater. Environ. Sci. 6 (4) (2015) 1147-1155
ISSN : 2028-2508
CODEN: JMESCN

Comparative study of low carbon steel corrosion inhibition in 200 ppm NaCl by amino acid compounds

O. Kassou[1*], M. Galai[1], R. A. Ballakhmima[1], N. Dkhireche[1], A. Rochdi[1], M. Ebn Touhami[1], R. Touir[1,2], A. Zarrouk[3]

1- Laboratoire des Matériaux, Electrochimie et Environnement, Faculté des Sciences, Université Ibn Tofail, BP 133, Kénitra 14000, Morocco.
2- Centre Régional des métiers de l'éducation et de la formation (CRMEF), Avenue Allal Al Fassi, Madinat Al Irfane, BP 6210 Rabat, Morocco.
3- LCAE-URAC18, Faculte des Sciences, Université Mohammed Premier, B.P. 717, 60000 Oujda, Morocco

Received 12 Oct 2014, revised 17 Nov 2014, Accepted 17 Nov 2014
**Corresponding author. E-mail address: o.kassou@gmail.com, Tel.: +212 661541371; Fax: +212 5 35 51 59 35.*

Abstract
The amino acid compounds have been tested as corrosion inhibitors for low carbon steel in a 200 ppm NaCl solution using potentiodynamic polarization curves and electrochemical impedance spectroscopy (EIS). Potentiodynamic polarization curves showed that these compounds act as cathodic-type inhibitors. Their inhibition efficiency (η) depends on the number of heteroatoms in their structure. This result was confirmed by the electrochemical impedance spectroscopy measurements. In addition, the impedance diagrams were composed of two capacitive loops badly separated. The first loop was attributed to the formation of a protective layer while the second was attributed to the charge transfer resistance. Finally, it is proved that the inhibition performance of Guanine was indeed improved by immersion time and reached a maximum of 96 % at 4 h.

*Keywords***:** amino acids; Corrosion inhibition; NaCl; low carbon steel; heteroatom number; Electrochemical measurements.

1. Introduction
Corrosion processes have an enormous economic impact as they involve the deterioration of metallic surfaces. Significant scientific and technological efforts have been made to control this phenomenon. Yet, the resort to chemical additives to inhibit the development of these corrosion processes remains at the top of the list. Most of the well-known inhibitors are organic compounds containing nitrogen, sulphur, and oxygen atoms. Indeed, compounds with functional groups containing hetero-atoms that can donate lone pair electrons are proved to be particularly useful as corrosion inhibitors for metals **[1-4].** These compounds are still continuously investigated as corrosion inhibitors for metals in industry. The selection criteria of the various inhibitors include low concentration, stability in recirculation, and cost effectiveness. Particularly, fatty amines associated with phosphonocarboxylic acid salts were the standard corrosion inhibitors [**5**]. Other researchers focused on the synergy between molybdate and other organic and inorganic compounds for corrosion and scale inhibition for water treatment in cooling water systems [**2, 3**]. As a result, the current trend for inhibitors use is towards more environmentally-friendly / eco-friendly / 'green' chemicals. Hence, we have studied, in a recent paper [**6, 7**], the effect of sodium gluconate anion as an effective non-toxic corrosion and scale inhibitor for low carbon steel in simulated cooling water. Other investigations on gluconate and gluconic acid as well as sodium, calcium and zinc salts of gluconic acid have been reported to be successful inhibitors against tin, iron and mild steel corrosion in near neutral media and in simulated cooling water [**8, 9**].
The aim of the present work is to electrochemically study the effect of the hetero-atoms number in the amino acids on the corrosion inhibition for low carbon steel in 200 ppm NaCl. The effect of immersion time, temperature and chloride ions on the performance of the best inhibitors was studied.

2. Experimental procedures
2.1. Electrochemical cell and materials
The electrolysis cell was a borosilicate glass (Pyrex®) cylinder closed by a cap with five apertures. Three of them were used for the electrode insertions. The working electrode was a low carbon steel previously used **[2, 6,7, 10]**

and its composition is summarized in Table 1. The surface area investigated was 0.8 cm^2. Prior to immersion test, the electrode was abraded using emery paper up to 1200 grade, cleaned with acetone, washed with distilled water, and finally dried up. Pt plate was used as the counter electrode while an Ag/AgCl electrode as the reference electrode. All potentials are referred to this electrode.

The corrosive solution is 200 ppm of NaCl. The temperature was adjusted at 32 ± 2 °C except for the study of the temperature effect. The electrolyte was in contact with air without any purging of dissolved oxygen. The chemical structures of the amino acids are presented in Figure 1.

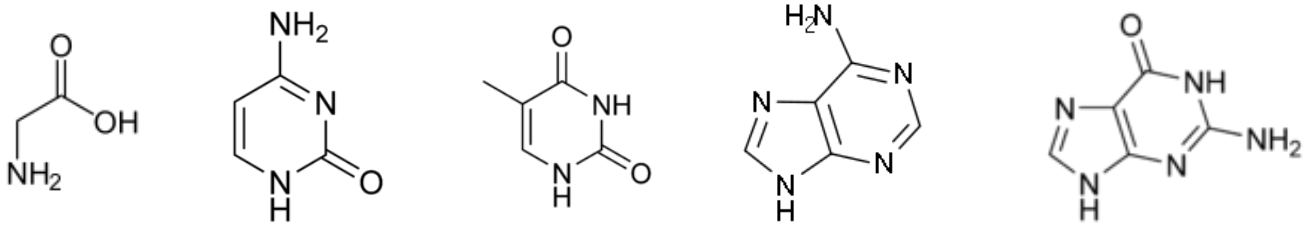

Glycine Cytosine Thymine Adenine Guanine

Figure 1. Molecular structures and names of the studied amino acids.

Table1. Composition of working electrode API 5L, elements other than **Fe**

Element	Ni	Si	C	Mn	S	P	Cr	Mo	V	Cu
%	0.02	0,31	0,45	0.71	0.019	0,017	0.06	0.01	0.01	0.01

2.2. Polarization measurements

The working electrode was immersed in test solution during half hour until the steady-state corrosion potential (E_{corr}) was reached. The cathodic polarization curve was recorded by polarization from E_{corr} towards more negative direction with a sweep rate of 1 mV/s. After this scan, the same electrode was kept in solution until the obtainment of the steady-state corrosion potential (E_{corr} ± 0.002 V), and then the anodic polarization curve was recorded from E_{corr} to positive direction with the same sweep rate. The obtained polarization curves were corrected for ohmic drop with the electrolyte resistance determined by electrochemical impedance spectroscopy. These measurements were carried out using a Potentiostat/Galvanostat/Voltalab PGZ 100 monitored by a personal computer. For each concentration, three independent experiments were conducted. The mean values and standard deviations are reported as well.

The overall current density values, *i*, were considered as the sum of two contributions, anodic and cathodic s i_a and i_c, respectively. For the potential domain not too far from the open circuit, it may be considered that both processes follow the Tafel law [**11**]. Thus, it can be derived:

$$i = i_a + i_b = i_{corr} \times \left\{ exp\left[b_a \times \left(E - E_{corr} \right) \right] - \exp\left[b_c \times \left(E - E_{corr} \right) \right] \right\} \qquad (1)$$

where i_{corr} is the corrosion current density (A cm^{-2}), b_a and b_c are the Tafel constants of the anodic and cathodic reactions (V^{-1}), respectively. These constants are linked to the Tafel slope β (V/dec) in usual logarithmic scale by:

$$\beta = \frac{\ln(10)}{b} = \frac{2.303}{b} \qquad (2)$$

The corrosion parameters were then evaluated by means of nonlinear least squares method by applying this equation using Origin software. However, for this calculation, the potential range applied was limited to ±0.100V around the E_{corr} else a significant systematic divergence was sometimes observed in both anodic and cathodic branches. The inhibition efficiency (η) was calculated using the following equation:

$$\eta = \frac{i_{corr}^0 - i_{corr}}{i_{corr}^0} \times 100 \qquad (3)$$

where i_{corr}^0 and i_{corr} are the corrosion current density values in the absence and in the presence of inhibitor, respectively.

2.3. EIS measurements

The electrochemical impedance spectroscopy measurements were carried out using a transfer function analyzer (Voltalab PGZ 100, Radiometer Analytical), over the frequency range from 100 kHz to 0.01 Hz with 10 points

per decade. The applied amplitude of AC signal was 10 mV_{rms}. All experiments were conducted at the open circuit potential. The obtained impedance data were analyzed in term of equivalent electrical circuit using Bouckamp's program **[12].** The inhibition efficiency was evaluated from R_p (which is obtained from the diameter of the semicircle in the Nyquist representation) with the relationship:

$$\eta = \frac{R_p - R_p^0}{R_p} \times 100 \qquad (4)$$

where R_p^0 and R_p are the resistance polarization values in the absence and in the presence of the inhibitor, respectively.

3. Results and discussion

3.1. Corrosion inhibition:

In this study, we have tested the influence of amino acid compounds on the corrosion of low carbon steel in 200 ppm NaCl. The obtained results are shown in Figure 2. First of all, it can be noticed that the cathodic branches do not exhibit well-defined Tafel region. It is also noted that the presence of all compounds does not affect practically its kinetic process. Moreover, the polarization curve in the presence of amino acid indicates a shift in the corrosion potential toward more negative values of potential compared with the blank solution.

To yield a quantitative approach, i_{corr} and E_{corr} were evaluated from the experimental results using a user-defined function of "Non-linear least squares curve fitting" (Eq. (1)) of the graphic software (Origin, OriginLab). In all cases, the correlation factor R^2 is higher than 0.999, thus, indicating a reliable result.

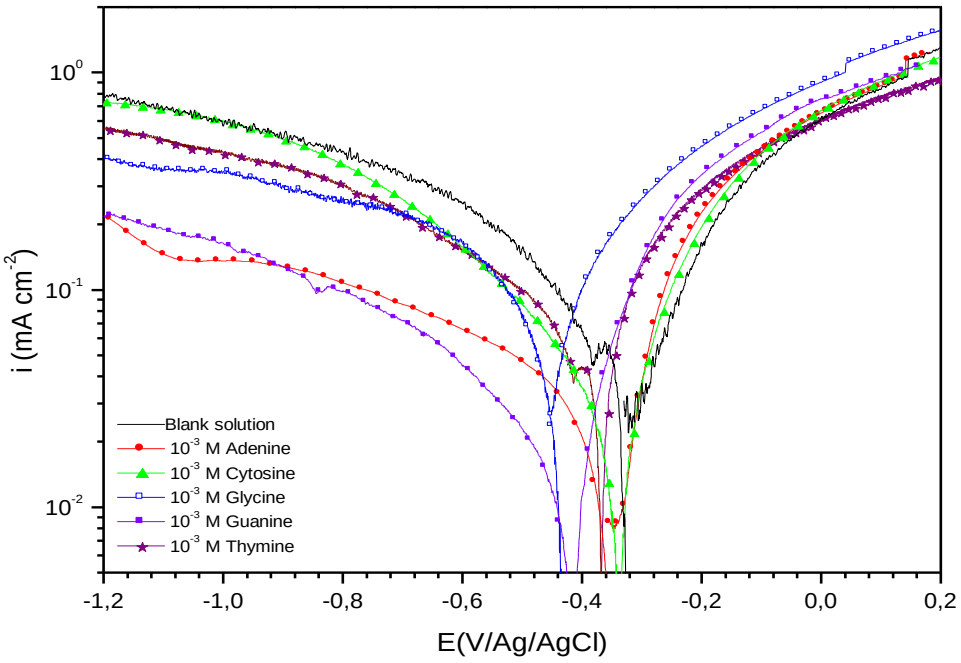

Figure 2: Potentiodynamic polarization curves of low carbon steel in 200 ppm NaCl in the presence of different compounds.

Table 2 summarizes the various corrosion kinetic parameters thus obtained. It can be noticed that the current densities decrease and the inhibition efficiency values increase by addition of inhibitors. This might be a possible proof that these compounds adsorb on the low carbon steel surface preventing it from corrosion. It can be also remarked that the cathodic and anodic Tafel slopes (β_a and β_c) values change with inhibitor addition indicating a change in the oxygen reduction and iron dissolution mechanism. In addition, the inhibition efficiency follows the following order: Guanine> Adenine> Cytosine> Thymine> Glycine. This order can be explained by the heteroatoms' number on these compounds (Table 2). In fact, the Guanine has six hetero-atoms and its inhibition is

greater than the Adenine which has five hetero-atoms. In addition, the last compounds are greater than Cytosine and Thymine as they have four hetero-atoms only. So when we compare, the Cytosine with Thymine, we notice that the inhibition efficiency depends on the nature of hetero-atoms. In fact, Cytosine has three nitrogen atoms and one oxygen atom whereas the Thymine has two – N atoms- and two –O- atoms, and we know indeed that the inhibition efficiency of the compounds that contain –N- in their structure is greater than that of those which contain the –O- atoms.
Generally the compounds containing heteroatoms like O, N, S, and P are found to work as very effective corrosion inhibitors. The efficiency of these compounds depends upon electron density present around the heteroatoms, the number of adsorption active centers in the molecule and their charge density, molecular size, mode of adsorption, and formation of metallic complexes [**13-16**]. According to these results, it is noted that the performance of amino acids depends on the nature and number of heteroatoms.

Table 2. Data obtained from polarization curves for low carbon steel in 200 ppm NaCl in the presence of different amino acids.

	heteroatoms number	E_{corr} (mV/Ag/AgCl)	i_{corr} (µA cm^{-2})	β_a (mV/dec)	β_c (mV/dec)	η%
Blank solution	-	-325	104	143	-287	-
10^{-3} M of Guanine	6 (5N-1O)	-415	9	144	-347	91
10^{-3} M of Adenine	5 (5N)	-350	18	156	-667	82
10^{-3} M of Cytosine	4 (3N-1O)	-338	30	205	-441	71
10^{-3} M of Thymine	4 (2N-2O)	-376	41	217	-231	60
10^{-3}M of Glycine	3 (1N-2O)	-430	65	403	-617	38

3.2. Electrochemical impedance spectroscopy:
In order to confirm the obtained results by potentiodynamic polarisation measurements and gather some information about the inhibition effect of amino acids, the electrochemical impedance spectroscopy was also used. The advantage of this method is that both the polarization resistance values and the double layer capacitance values can be obtained in the same measurement.
Figure 3 gives the EIS spectra of low carbon steel in 200 ppm NaCl solution without and with 10^{-3} M of each compound. The complex plane plots reveal the presence of two slightly depressed semicircles their diameters correspond to the polarization resistance whose value increases with the addition of amino acids. A simple electrical equivalent circuit (Figure 4) has been proposed to model the experimental data. The employed circuit allowed the identification of solution resistance (R_s), charge transfer resistance (R_{ct}) and resistance associated with the layer of products formed (R_f). It is noteworthy that the double layer capacitance (C_{ct}) value was affected by imperfections of the surface, and this effect was simulated via a constant phase element (*CPE*) [**17, 18**]. Considering the roughness and inhomogeneity of the solid electrode surface, here, the constant phase elements CPE_f and CPE_{ct} are used to replace the film capacitance and the double layer capacitance respectively, and their values can be assessed by the following equation (4) [**19, 20**]:

$$Z_{CPE}(\omega) = Y^{-1}(j\omega)^{-n} \quad (5)$$

where, *Y* is the *CPE* constant, ω is the sine wave modulation angular frequency (in rad s^{-1}), $j^2=-1$ is the imaginary number and *n* is the *CPE* exponent. Depending on *n*, *CPE* can represent resistance [$Z_{CPE} = R$, $n = 0$], capacitance [$Z_{CPE} = C$, $n = 1$], inductance [$Z_{CPE} = L$, $n = -1$] or Warburg impedance for ($n = 0.5$) [**21**].
In addition, Hirschorn and al. [**22**] recently reported that the effective capacity C can be estimated using the following mathematical formulas from the CPE [**23, 24**]:

$$C = Q^{\frac{1}{\alpha}} \times R^{\frac{(1-\alpha)}{\alpha}} \quad (6)$$

According to the fitting results in Table 3, the inhibition efficiency values increase with the presence of amino acid. The values of charge transfer resistance R_{ct} increase with the addition of inhibitors which indicates the insulated adsorption layer's formation. Moreover, this increase in R_{ct} is observed after addition of each inhibitor. This phenomenon indicates that the charge transfer process is impeded when the uncovered area available for this process is diminished. This can be explained by the adsorption of amount of inhibitors molecules at the metal /electrolyte interface. It can be observed that the film capacitance in the absence of inhibitors is larger than in its presence in the case of Cytosine, Glycine or Guanine. The addition of inhibitors in the test solution leads to a

decrease of the double layer capacitances because the inhibitor molecules adsorb at the inner Helmholtz plane and block the active sites on the metal surface. In addition, it is noted that resistance electrolyte R_s change with amino acids addition. This can be explained by the change in the pH solution after inhibitors addition.

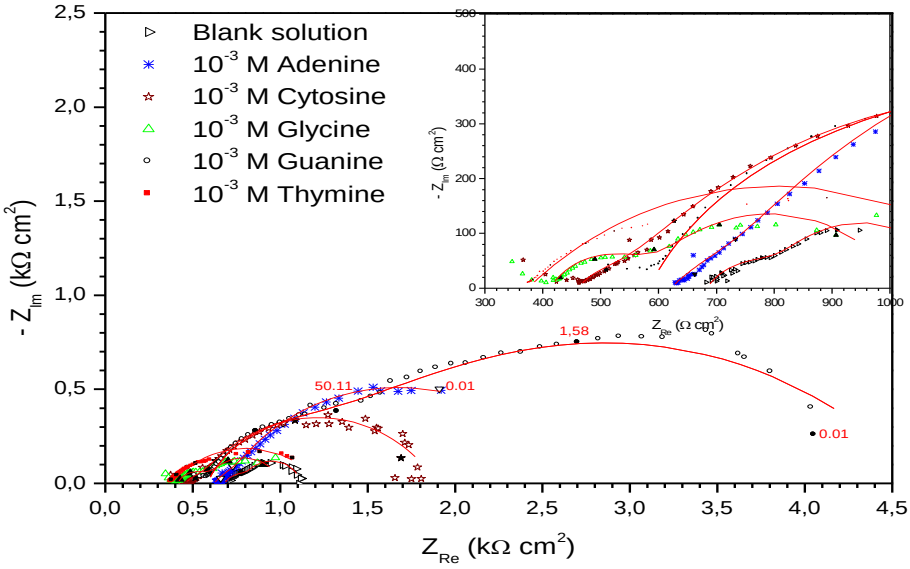

Figure 3: Nyquist plots obtained for low carbon steel in 200 ppm NaCl with and without 10^{-3} M of amino acids. Symbols: Experimental data and Red continuous lines: Fitting data.

However, these obtained results confirm those funded by potentiodynamique polarization curves and the inhibition efficiency follows the following order: Guanine> Adenine> Cytosine> Thymine> Glycine

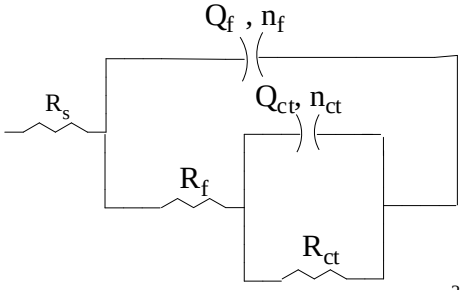

Figure 4. Nyquist plots of low carbon steel in 200 ppm NaCl containing 10^{-3} M of amino acid at E_{corr}

Table 3. Electrochemical parameters for low carbon steel in 200 ppm NaCl with and without 10^{-3} M of amino acids.

	heteroatoms number	R_s [a]	R_f [a]	C_f [b]	n_f	R_{ct} [a]	C_{ct} [b]	n_{ct}	R_p [a]	η□%
Blank solution	-	682.1	0.27	182.6	0.62	0.67	2630	0.82	0.26	-
Guanine	6 (5N-1O)	582.8	0.78	0.65	0.72	3.32	42.95	0.49	3.52	93
Adenine	5 (5N)	621.1	0.41	403.4	0.53	1.73	476.3	0.77	1.52	83
Cytosine	4 (3N-1O)	461.2	0.43	13.26	0.62	1.31	170.9	0.59	1.28	79
Glycine	4 (2N-2O)	420.8	0.40	0.27	0.68	0.50	193	0.71	0.48	46
Thymine	3 (1N-2O)	373.5	0.12	324.8	0.49	0.83	100.4	0.39	0.58	45

[a] R_s is expressed in Ω cm^2 while R_f , R_{ct} and R_p are expressed in kΩ cm^2
[b] C_f and C_{ct} are given in µF cm^{-2}

3.3. Influence of immersion time on the performance of Guanine:

The effect of immersion time on the Guanine performance of low carbon steel in 200 ppm NaCl solution is shown in Figure 5. The Nyquist plots consisted of two capacitive loops. The one at high frequency was attributed to the adsorbed film resistance due to adsorption of the inhibitors molecules and all other accumulated products.

Conversely, the one at low frequency was usually attributed to the double layer capacitance and the charge transfer resistance. It is noted also that the impedance spectra reported in Figure 6 shows an increase of the total impedance (the diameter of impedance from high frequency to low frequency) of the system with immersion time from ½ h to 2 h. This evolution suggests a strong inhibition of the dissolution processes occurring on the surface **[25, 26]**. The equivalent circuit shown in Figure 5 was used to simulate the impedance spectra. The relevant impedance parameters obtained by regression calculation are shown in Table 4. Simultaneously the C_{ct} values decrease with immersion time. Water molecules that are present on metal/solution interface possess a higher value of the relative dielectric constant. When water molecules are replaced by inhibitor molecules, a decrease in the C_f value occurs [**27**].
However, in a 4 h to 12 h immersion time, the polarization resistance decreases. This evolution suggests that Guanine becomes low attached on the metal surface.

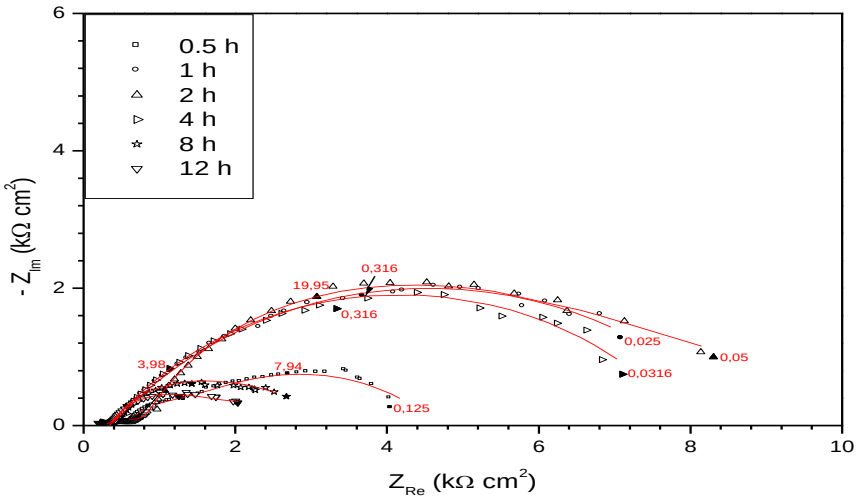

Figure 5. Nyquist plots obtained for low carbon steel in 200 ppm NaCl with and without 10^{-3} M of Guanine. Symbols: Experimental data and Red continuous lines: Fitting data.

Table 4. Electrochemical parameters of low carbon steel in 200 ppm NaCl containing 10^{-3} M of Guanine at different immersion time.

	R_s [a]	R_f [a]	C_f [b]	n_f	R_{ct} [a]	C_{ct} [b]	n_{ct}	R_p [a]	η%
0.5	582.8	0.78	0.65	0.72	3.32	42.95	0.49	3.52	93
1	175.5	0.21	0.43	0.50	8.36	104.9	0.57	8.39	97
2	311.6	1.05	0.56	0.22	10.85	38.54	0.76	11.59	98
4	341.2	1.68	7.5	0.59	7.51	3.5	0.59	7.33	96
8	220.4	0.32	3.7	0.39	2.93	53.09	0.84	3.03	91
12	233.3	0.59	210	0.12	1.71	68.48	0.75	2.07	87

[a] R_s is expressed in Ω cm^2 while R_f , R_{ct} and R_p are expressed in kΩ cm^2
[b] C_f and C_{ct} are given in µF cm^{-2}

3.4. Effect of solution temperature:
The effect of solution temperature on the corrosion inhibition efficiency of 10^{-3} M of Guanine, was studied in a temperature interval of 305 K to 325 K in 200 ppm NaCl solution. This temperature range was selected since in cooling systems the water temperature may reach 333 K. Figure 6 shows the corresponding results of the Nyquist plots obtained at E_{corr}. These plots consisted of two capacitive loops. The one at high frequency was attributed to the adsorbed film resistance and the one at low frequency was usually attributed to the double layer capacitance and the charge transfer resistance. It is noted also that the impedance spectra reported in Figure 6 shows that the total impedance of the system decreases due to temperature.
Table 5 summarizes the values of polarization resistance extracted from EIS at various temperatures. According to Gomma **[28]**, the kinetic of such corrosion acquires the character of a diffusion process in which the quantity of inhibitor present on the metal surface is greater at a lower temperature than that at a higher temperature. The

results show that the inhibition efficiency decreases with temperature indicating that at higher temperatures a dissolution of low carbon steel predominates in inhibitor adsorption. This could be explained on the basis of the temperature-dependent Guanine adsorption/desorption processes. For example, with an increase in temperature, the Guanine molecules adsorption equilibrium could shift towards the desorption process, resulting in a lower surface coverage [**29, 30**]. This would also result in a decrease in the Guanine molecules surface conformation order and, thus, a decrease in the protection against corrosive ions. Nevertheless, the corrosion inhibition efficiency was relatively high, even at 305-325 K range.

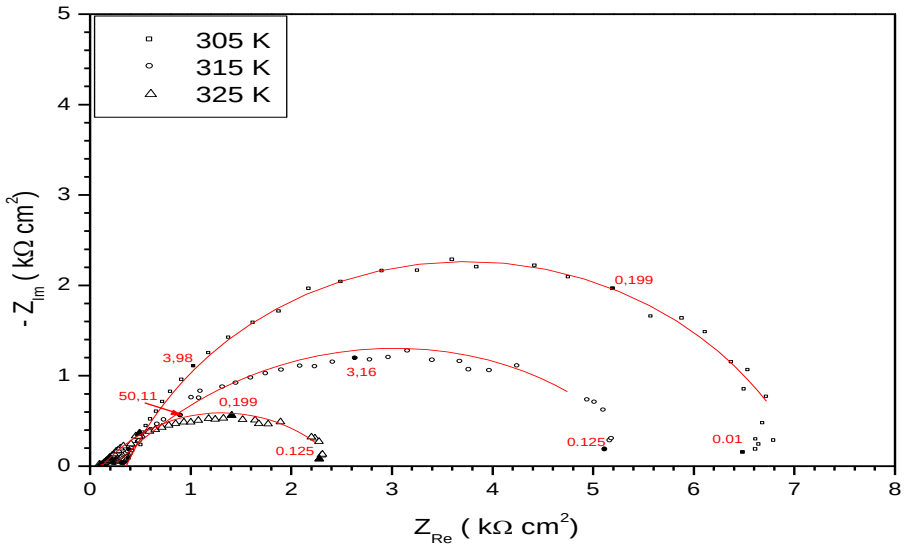

Figure 6: Effect of the solution temperature on the Nyquist plots of low carbon steel in 200 ppm NaCl with 10^{-3} M of Guanine. Symbols: Experimental data and Red continuous lines: Fitting data.

Table 5. Electrochemical parameters of low carbon steel in in 200 ppm NaCl with 10^{-3} M of Guanine at various temperatures.

T (K)	R_s [a]	R_f [a]	C_f [b]	n_f	R_{ct} [a]	C_{ct} [b]	n_{ct}	R_p [a]	η
305	370.7	5.20	37.25	0.81	1.37	284	1	6.20	96
315	234.9	1.77	59.94	0.53	3.30	253	0.18	4.83	95
325	113.9	0.19	85.98	0.57	2.14	539	0.39	2.22	88

[a] R_s is expressed in Ω cm^2 while R_f , R_{ct} and R_p are expressed in kΩ cm^2
[b] C_f and C_{ct} are given in µF cm^{-2}

3.4. Effect of Cl- ions in the performance of Guanine :

In order to evaluate the inhibition potential of the Guanine, we choose another more aggressive medium such as 3 % NaCl. The Nyquist plots were carried out in turn to characterize the corrosion behaviour of low carbon steel immersed for 1/2 h, at free corrosion potential, in 3% NaCl medium with and without 10^{-3} M of Guanine. The results are shown in Figure 7. These plots show two loops. The high frequency (HF) loop shows a linear portion having a slope close to 50° (which can be viewed on the HF zoom in the right Figure), suggesting the existence of a porous behaviour in agreement with de Levie theory [**31**]. However, the second loop is assigned to the double layer capacitance and the charge transfer resistance. The equivalent circuit proposed is shown in Figure 8. Where R_s indicates the electrolyte resistance; R_f is the resistance associated with the layer of products formed; R_{ct} corresponds to the charge transfer resistance; C_{ct} is associated to the double-layer capacitance and W_d is the diffusion impedance through the Nernst layer of products formed. So, the Warburg element for convective diffusion is equivalent to the Warburg element in the high frequency range. $(f >> \frac{2.54}{2\pi\tau_d})$. However, it is noted that the impedance spectra shows a decrease in the total impedance of the system with the addition of 10^{-3} M of Guanine. The electrochemical parameters summarized in Table 5, show that the addition of 10^{-3} M of Guanine

provides an acceleration of corrosion. This proves that the Guanine doesn't keep up to its performance in a very aggressive solution due to the aggressivety of Cl^- ions.

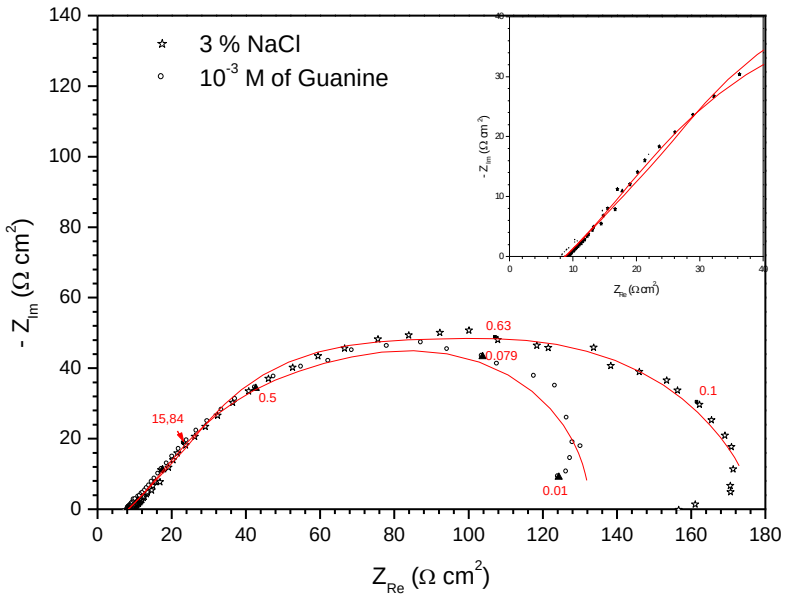

Figure 7: EIS diagrams of low carbon steel in 3 % NaCl solution with and without 10^{-3} M of Guanine. Symbols: Experimental data and Red continuous lines: Fitting data.

Table 6. Electrochemical parameters of low carbon steel in 3 % NaCl with 10^{-3} M of Guanine.

	R_s [a]	τ_d [b]	R_f [a]	R_{ct} [a]	C_{ct} [b]	n_{ct}	R_p [a]	η
3 % NaCl	8.24	0.169	88.3	113.3	4.05	0.82	193	-
Guanine	8.11	6.01	67	87.3	173	0.85	146	- 32

[a] R_f , R_{ct} , R_s and R_p are expressed in Ω cm^2
[b] C_{ct} are given in mF cm^{-2} and the τ_d is given in S

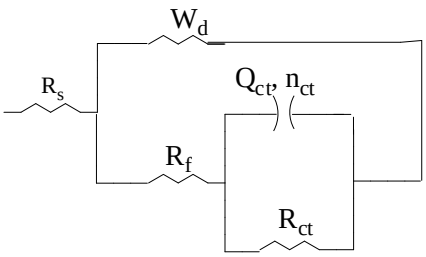

Figure 8: Equivalent circuit models used to fit the experiment impedance data.

Conclusion

Amino acids are cathodic corrosion inhibitors for low carbon steel in 200 ppm NaCl solution. The obtained inhibition efficiency depends on the nature and the heteroatoms number. So, the Guanine containing six heteroatoms has proved to be the best. Moreover, the inhibition efficiency of Guanine increases with immersion time ranging from ½ to 2 h and decreases beyond this value until 12 h. In addition, the best inhibitor doesn't perform efficiently at height temperatures and in a more aggressive medium. These results show that a layer of corrosion products forms naturally on the low carbon steel surface and its occurrence in these systems evolves over time. Finally, we were able to ascertain that the alteration of the layer formed on the metal surface depends on the molecular structure of the inhibitor.

References

1. Tourabi K., Nohair K., Nyassi N., Hammouti B., Bentiss F., Chetouani A., *Mor. J. Chem.*,1 (2013) 33-46
2. Cenoui M., Dkhireche N., Kassou O., Ebn Touhami M., Touir R., Dermaj A., Hajjaji N., *J. Mater. Environ. Sci.*, 1 (2010) 84-95.
3. Labriti B., Dkhireche N., Touir R., Ebn Touhami M., Sfaira M., El Hallaoui A., Hammouti B., Alami A., *Arab. J. Sci. Eng.*, 37 (2012) 1293–1303
4. Boudalia M., Bellaouchou A., Guenbour A., Bourazmi H., Tabiyaoui M., El Fal M., Ramli Y., Elmsellem H., *Mor. J. Chem.*, 2 (2014) 97-109.
5. Marin-cruz J., Cabrera-Sierra R., Pech-Canul M.A., Gonzàlez I., *Electrochem. Acta* (2005).
6. Touir R., Dkhireche N., Ebn Touhami M., Lakhrissi M., Lakhrissi B., Sfaira M., *Desalination* 249 (2009) 922–928.
7. Touir R., Cenoui M., El Bakri M., Ebn Touhami M., *Corrosion Science* 50 (2008) 1530–1537
8. Puckorius P.R., Strauss S.D., *Power* 5 (1995) 17.
9. Telegdi J., Kàlmàn E., Kàrmàn F.H., *Corros. Sci.* 33 (1992) 1099.
10. Dkhireche N., Dahami A., Rochdi A., Hmimou J., Touir R., Ebn Touhami M., El Bakri M., El Hallaoui A., Anouar A., Takenouti H., *Journal of Industrial and Engineering Chemistry* 19 (2013) 1996–2003.
11. Stern M., Geary A.L., *J. Electrochem. Soc.*, 104 (1957) 56-63
12. Bouckamp A., Users Manual Equivalent Circuit, Ver. 4.51, 1993.
13. Derya Lec H., Emregu K. C., Atakol O., *Corros. Sci.*, 50 (2008) 1468-1474
14. Quraishi M. A., Singh A., Singh V. K., Yadav D. K., Singh A. K., *Mater. Chem. Phys.*, 122 (2010) 114-122.
15. Singh A., Ahamad I., Singh V. K., Quraishi M. A., *J. Solid State Electrochem.*, 15 (2011) 1087-1097.
16. Oguzie E.E., Oguzie K. L., Akalezi C. O., Udeze I. O., Ogbulie J. N., Njoku V. O., *Sustain. Chem. Eng.*, 1 (2013) 214-225.
17. Benabdellah M., Souane R., Cheriaa N., Abidi R., Hammouti B., Vicens J., *Pigment and Resin Technology*, 36 (2007) 373–381.
18. Popova A., Christov M., *Corros. Sci.*, 48 (2006) 3208–3221
19. Wang X., Yang H., Wang F., *Corros. Sci.*, 52 (2010) 1268-1276.
20. Salasi M., Shahrabi T., Roayaei E., Aliofkhazraei M., *Mater. Chem. Phys.*, 104 (2007) 183-190.
21. Tsuchiya H., Fujimoto S., Chihara O., Shibata T., *Electrochim. Acta*, 47 (2002) 4357-4366.
22. Hirschorn B., Orazem M.E., Tribollet B., Vivier V., Frateur I., Musiani M., *Electrochim. Acta*, 55 (2010) 6218
23. Hsu C.H., Mansfeld F.. *Corrosion* 57 (2001) 747.
24. Brug G.J., Van Den Eeden A.L.G., Sluyters-Rehbach M., Sluyters J.H., *J. Electroanal. Chem.*, 176 (1984) 275.
25. Jamil H.E., Shriri A., Boulif R., Bastos C., Montemor M.F., Ferreira M.G.S., *Electrochim. Acta*, 49 (2004) 2753-2760.
26. Bommersbach P., Alemany-Dumont C., Millet J.P., Normand B., *Electrochim. Acta*, 51 (2005) 1076–1084.
27. Souza F.S., Spinneli A., *Corros. Sci.*, 51 (2009) 642-649.
28. Gomma G. K., *Mater. Chem. Phys.*, 56 (1998) 27-34.
29. Bouklah M., Hammouti B., Lagrenée M., Bentiss F., *Corros. Sci.*, 48 (2006) 2831–2842.
30. Popova A., Christov M., Vasilev A., *Corros. Sci.*, 49 (2007) 3290–3302.
31. de Levie R., Electrochemical response of protons and rough electrodes, in: Dclahay P., Tobias G.W. (Eds.), Advances in Electrochemistry and Electrochemical Engineering, vol. 6, Wiley, New York, 1967, p. 329.